Available online at www.sciencedirect.com

ScienceDirect

Procedia Manufacturing 10 (2017) 183 – 193

Procedia MANUFACTURING

45th SME North American Manufacturing Research Conference, NAMRC 45, LA, USA

A Study of Milling Surface Quality during Period-2 Bifurcations

Andrew Honeycutt and Tony L. Schmitz*

University of North Carolina at Charlotte, Charlotte, NC, 28223, USA

Abstract

This paper provides time domain simulation and experimental results for surface location error and surface roughness when machining under both stable (forced vibration) and unstable (period-2 bifurcation) conditions. It is shown that the surface location error follows similar trends observed for forced vibration, so zero or low error conditions may be selected even for period-2 bifurcation behavior. The surface roughness for the period-2 instability, on the other hand, is always larger than for stable conditions because the surface is defined by every other tooth passage and the apparent feed per tooth is subsequently increased. Good agreement is observed between simulation and experiment for stability, surface location error, and surface roughness results.

© 2017 The Authors. Published by Elsevier B.V. This is an open access article under the CC BY-NC-ND license (http://creativecommons.org/licenses/by-nc-nd/4.0/).
Peer-review under responsibility of the organizing committee of the 45th SME North American Manufacturing Research Conference

Keywords: Milling, dynamics, chatter, bifurcation, surface location error, surface roughness

1. Introduction

Research in machining dynamics and instability covered more than seven decades. In 1946 Arnold analyzed tool vibration during steel machining [1]. Follow-on work used time-delay differential equations to describe the self-excited vibrations (chatter) that can occur when machining [2], identified regeneration of surface waviness from one revolution (turning) or tooth (milling) to the next as the feedback mechanism that also defines the time delay [3-6], and provided analytical algorithms to predict stable and unstable cutting conditions [4-12]. In 1998, approximately 50 years after Arnold's paper, Davies et al. measured period-n milling bifurcations, which complemented the traditional secondary (subcritical) Hopf bifurcation that had been previously studied [13]. This research led to

* Corresponding author. Tel.: +1-704-687-5086.
E-mail address: tony.schmitz@uncc.edu

2351-9789 © 2017 The Authors. Published by Elsevier B.V. This is an open access article under the CC BY-NC-ND license (http://creativecommons.org/licenses/by-nc-nd/4.0/).
Peer-review under responsibility of the organizing committee of the 45th SME North American Manufacturing Research Conference
doi:10.1016/j.promfg.2017.07.046

multiple publications that modeled and predicted both the secondary Hopf and period-n behavior with a focus on the period-2 and period-3 cases [14-18]. Recently, Honeycutt and Schmitz presented the extended milling bifurcation diagram that revealed higher order period-n bifurcations at depths of cut well above the traditional stability limit [19]. They also predicted and experimentally validated period-2, -3, -6, -7, and -15 bifurcations for milling [20]. The sensitivity of period-n bifurcation behavior to the structural dynamics (natural frequency and damping) was studied both numerically and experimentally.

When stable machining conditions are selected, two additional considerations for high quality part manufacture are: 1) surface location error, or part geometric errors that occur due to forced vibrations; and 2) surface roughness. Surface location error, or SLE, has been modeled and predicted for stable milling conditions by several authors [21-28]. In these publications, the difference between the machined surface location and the commanded location is measured and/or predicted to determine the influence of (stable) machining conditions on the error. Similarly, surface roughness has been considered as an important quality metric for machined parts since it influences fatigue, sealing performance, wear, and aesthetics, for example. However, prior studies of period-n bifurcations (instabilities) have evaluated neither SLE nor surface roughness. The purpose of this paper is to predict and measure both quantities for stable and period-2 bifurcation behaviors. In the following sections the time domain simulation algorithm is described, a numerical example is provided, the experimental setup is detailed, and numerical and experimental results are presented for SLE and surface roughness when milling under both stable and period-2 bifurcation conditions.

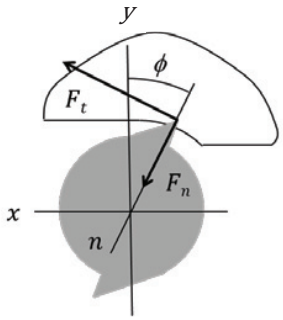

Fig. 1. Cutting force geometry. The normal and tangential direction cutting forces, F_n and F_t, are displayed. The fixed x (feed) and y directions, as well as the rotating normal direction, n, are also shown. The angle ϕ defines the tooth angle. The tool feed is to the right for the clockwise tool rotation and the axial depth is in the z direction.

Nomenclature

F_n	force in the normal direction
F_t	force in the thrust direction
r	endmill radius
ϕ	tooth angle
x	feed direction
y	perpendicular to feed direction in plane of the cut
z	tool axis direction
f_t	feed per tooth
N_t	number of teeth on the endmill
SR	steps per revolution in the time domain simulation
Ω	spindle speed (rpm)
b	axial depth of cut
SLE	surface location error

2. Time Domain Simulation

Time domain simulation enables the numerical solution of the coupled, time-delay equations of motion for milling in small time steps [29]. It is well-suited to incorporating the inherent complexities of milling dynamics, including the nonlinearity that occurs if the tooth leaves the cut due to large amplitude vibrations and complicated tool geometries (incorporating runout, or different radii, of the endmill teeth, non-proportional teeth spacing, and variable helix). The simulation is based on the Regenerative Force, Dynamic Deflection Model described by Smith and Tlusty [30]. As opposed to analytical stability maps that provide a global picture of the stability behavior, time domain simulation provides information regarding the local cutting force and vibration behavior for the selected cutting conditions.

Once the *x* and *y* direction displacements are determined by time domain simulation, the final spatial trajectory for each tooth is determined by summing these vibration-induced displacements with the nominal cycloidal motion of the teeth due to the combined translation and rotation. This final spatial trajectory is finally used to define the machined surface and, subsequently, to predict the SLE and surface roughness. The nominal cycloidal motion components in the *x* and *y* directions are defined by Eqs. 1 through 3, where *i* is the time step index, *df* is the linear feed per time step, *r* is the endmill radius, f_t is the commanded feed per tooth, N_t is the number of teeth, and *SR* is the number of steps per revolution in the time domain simulation.

$$x_{nom} = r \sin \phi + i \cdot df \tag{1}$$

$$y_{nom} = r \cos \phi \tag{2}$$

$$df = \frac{f_t \cdot N_t}{SR} \tag{3}$$

3. Numerical Example

To demonstrate stability, SLE, and surface roughness results obtained from time domain simulation, a numerical example is presented. The strategy of periodic sampling is applied to differentiate between stable machining and bifurcation behavior. The cutting conditions for the simulation are 5% radial immersion up (conventional) milling at 30000 rpm with a feed per tooth of 0.1 mm/tooth. The 8 mm diameter, 45 deg helix, single tooth tool has symmetric dynamics with a 721 Hz natural frequency, a viscous damping ratio of 0.009, and a 4.1×10^5 N/m stiffness. The aluminum workpiece cutting force coefficients are $\boldsymbol{k_{tc}}$ = 604×10^6 N/m^2 and $\boldsymbol{k_{nc}}$ = 223×10^6 N/m^2 (zero edge coefficients).

The tool vibration in the feed (*x*) direction for an axial depth of b = 0.5 mm is displayed in Fig. 2. For this stable cut the once-per-tooth sampled points (circles) repeat because stable cuts exhibit forced (synchronous) vibrations. The corresponding Poincaré map, which plots displacement versus velocity, is also included in Fig. 2. It is observed that a single point is obtained from the once-per-tooth (periodic) sampling. This identifies stable behavior that repeats with each tooth passage. Figure 3 shows results for b = 2.5 mm. This provides an example of period-2 behavior. In this case, the vibration repeats every other tooth passage, so two distinct points are visible in the Poincaré map. Secondary Hopf behavior is demonstrated in Fig. 4 with b = 5.0 mm. Here, the chatter frequency near the system natural frequency causes the quasi-periodic behavior and an elliptical distribution of points appears in the Poincaré map. This distribution is indicative of the traditional, secondary Hopf instability.

The spatial trajectory of the endmill tooth is displayed in Fig. 5. It includes both the nominal path and the vibrations due to the cutting force. Because this is up milling, the uppermost points define the machined surface (for down milling, it would be the lowermost points). The upper surface is shown in more detail in the inset. It is seen that the period-2 behavior causes the final surface to be defined by every other tooth passage. The trajectories with their apex at approximately 4006 μm produce the surface, while the alternating trajectories at approximately 3991 μm remove material, but do not affect the final surface details. In this case, the surface location error is 6 μm

because the 8 mm diameter (4 mm radius) tool should leave the surface at 4000 µm. This surface is overcut by 6 µm, i.e., more material is removed than commanded. The arithmetic average surface roughness for the profile is Ra = 0.3 µm.

For the selected system dynamics, the traditional stability limit (i.e., the transition from stable to any bifurcation behavior) at 30000 rpm is 0.77 mm. At the selected spindle speed, therefore, the optimum axial depth of cut would be 0.77 mm or less. If the 2.5 mm axial depth that resulted in period-2 behavior was chosen, a 325% increase in material removal rate would be achieved. Provided the 6 µm SLE and 0.3 µm Ra are acceptable for the selected application, this presents a compelling case for machining at the period-2 conditions.

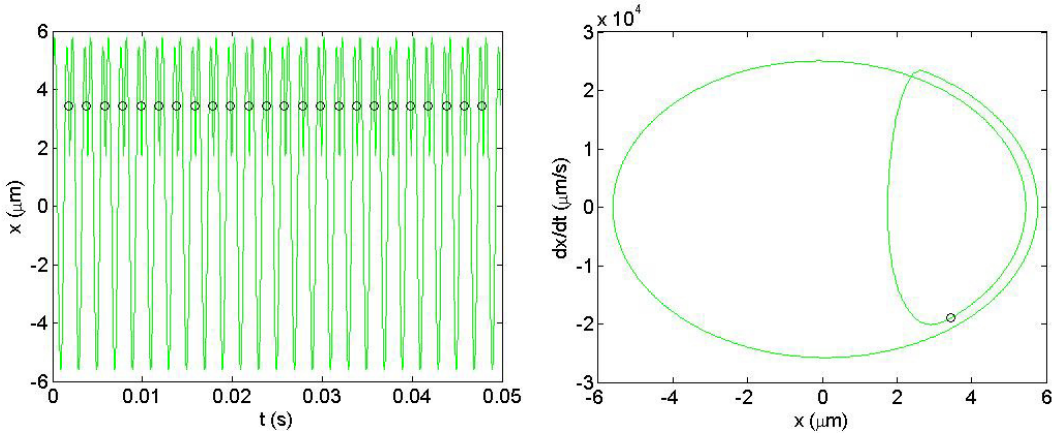

Fig. 2. (Left) Feed direction (*x*) vibration versus time with once-per-tooth sampled points (circles) for *b* = 0.5 mm. (Right) Poincaré map with once-per-tooth sampled points. Because the cut is stable, all sampled points appear at the same location.

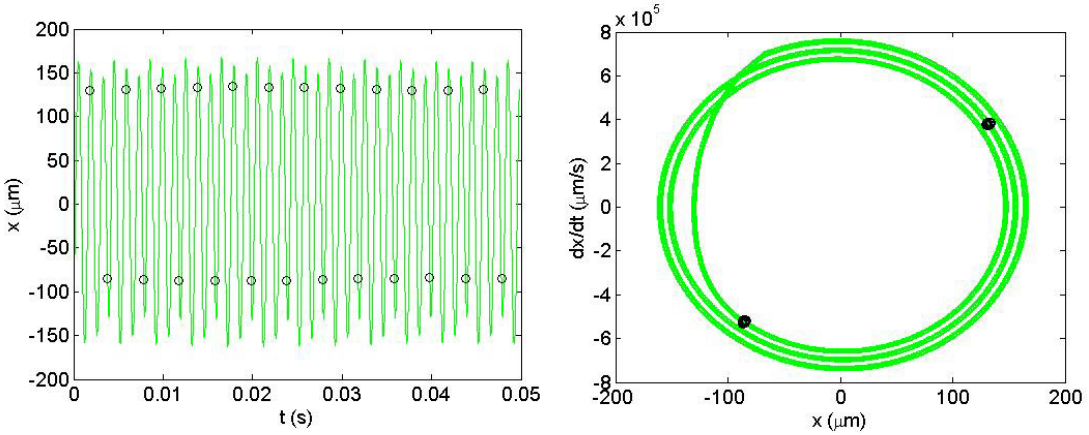

Fig. 3. (Left) Feed direction (*x*) vibration versus time with once-per-tooth sampled points (circles) for *b* = 2.5 mm. (Right) Poincaré map with once-per-tooth sampled points. The period-2 bifurcation behavior shows two sampled point locations. Because the solution alternates between two values, this is referred to as a flip bifurcation.

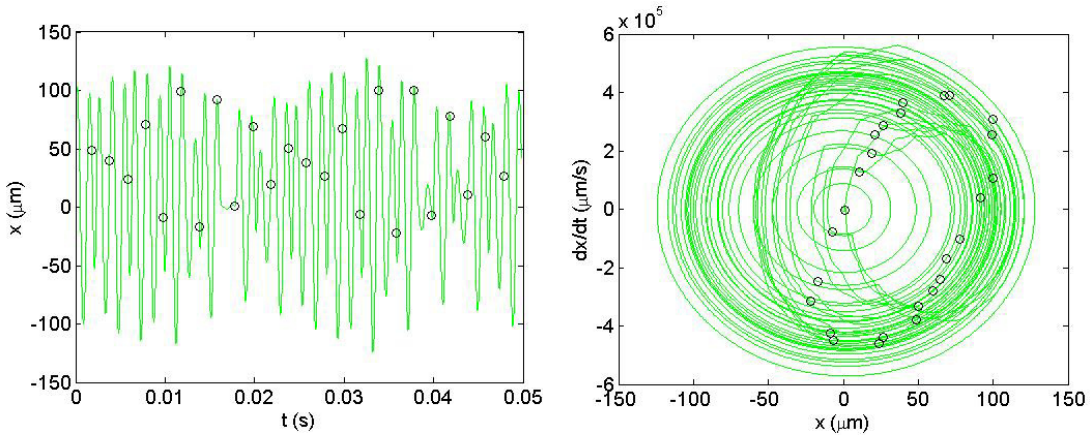

Fig. 4. (Left) Feed direction (x) vibration versus time with once-per-tooth sampled points (circles) for b = 5 mm. (Right) Poincaré map with once-per-tooth sampled points. The secondary Hopf instability yields an elliptical distribution of sampled points.

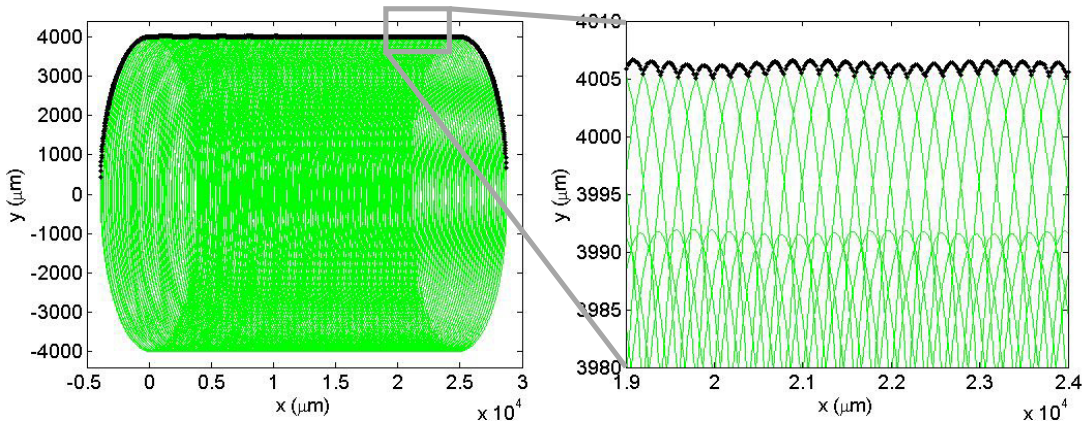

Fig. 5. (Left) Spatial trajectory of the endmill tooth for b = 2.5 mm. (Right) Magnified view of upper surface of tooth trajectory. The machined surface is defined by the points at the top of the trajectory for the up milling cut. The period-2 behavior gives upper and lower tooth paths. The upper path defines the final surface, although material is removed for each tooth passage.

4. Experimental Results

The flexure-based setup displayed in Fig. 6 was used to define a physical system for simulation and testing [31-32]. The setup included a parallelogram leaf-type flexure with an aluminum workpiece mounted on top. The in-process vibration data was collected using a laser vibrometer (velocity) and capacitance probe (displacement). Both were aligned with the flexible direction for the single degree of freedom flexure. Note that the feed direction is perpendicular to this flexible direction. This orientation was selected to emphasize variations in surface location error and surface finish with machining conditions. Once per tooth sampling was accomplished using a laser tachometer and reflective target attached to the rotating tool holder. The flexure dynamics were identified by modal testing: 125.8 Hz natural frequency, 0.0136 viscous damping ratio, and 1.75×10^6 N/m stiffness in the flexible (feed) direction. The dynamics for the 19.1 mm diameter, 0 deg helix angle tool (one insert, ISO SPEB090308, ANSI SPEB322, Kennametal 1157544, grade KC730) were symmetric: 1188 Hz natural frequency, 0.095 viscous damping ratio, and 4.24×10^7 N/m stiffness. The 6061-T6 aluminum alloy cutting force coefficients were: k_{tc} =

770×10^6 N/m^2, k_{nc} = 368×10^6 N/m^2, k_{te} = 22×10^3 N/m, and k_{ne} = 22×10^3 N/m. The up milling cutting conditions were: 5 mm axial depth, 2 mm radial depth, 0.35 mm/tooth, and variable spindle speed. Spindle speed values were selected to span from period-2 to stable cutting conditions while holding all other parameters constant. These spindle speeds and the corresponding behavior are listed in Table 1.

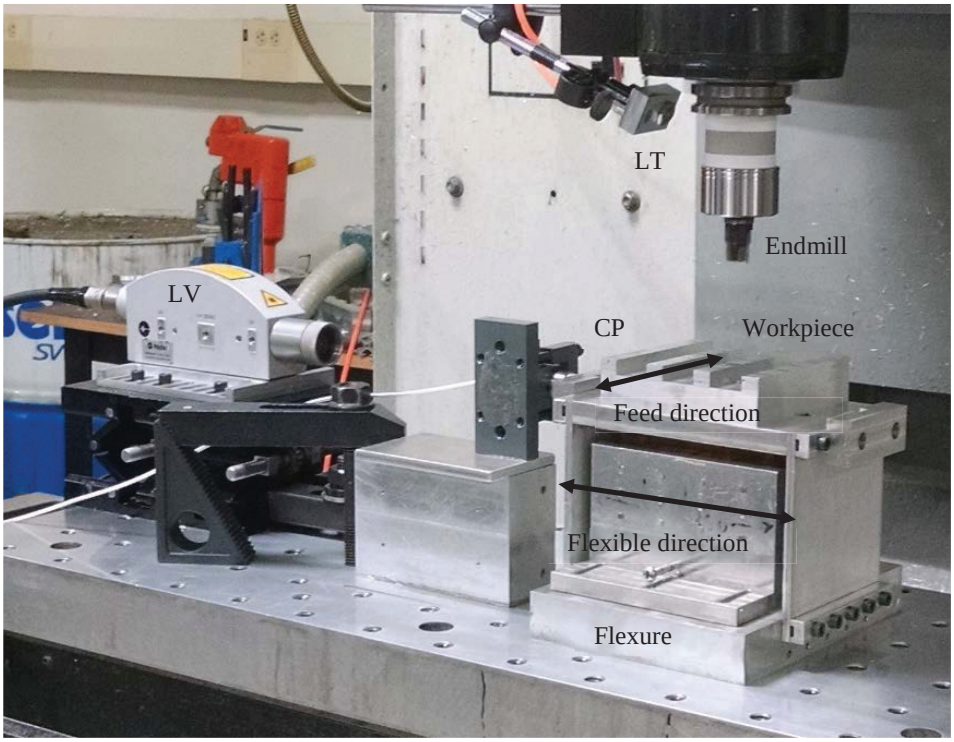

Fig. 6. Flexure-based experimental setup with laser vibrometer (LV), laser tachometer (LT), and capacitance probe (CP). The feed direction and the flexible direction for the flexure are also identified.

Table 1. Spindle speeds and bifurcation behavior for experiments.

Spindle Speed (rpm)	Behavior	Spindle Speed (rpm)	Behavior
3180	Period-2	3330	Stable
3190	Period-2	3360	Stable
3200	Period-2	3400	Stable
3210	Period-2	3500	Stable
3270	Stable	3600	Stable
3300	Stable		

The workpiece geometry is presented in Fig. 7. The initial ribs were machined directly on the flexure so it could be ensured that the part was aligned with the machine axes. Low axial and radial depths were selected to minimize vibration levels and the same conditions were used to machine each rib. Prior to beginning the SLE/Ra experiments, a test workpiece was machined and the four ribs were measured on a coordinate measuring machine (CMM) to evaluate the repeatability of the starting rib dimensions. The mean value was 9.82 mm with a standard deviation of

2.8 µm. Given the adequate repeatability of the initial ribs, the 11 spindle speeds in Table 1 were used to machine 11 ribs (three total workpieces). All machining conditions were identical other than spindle speed.

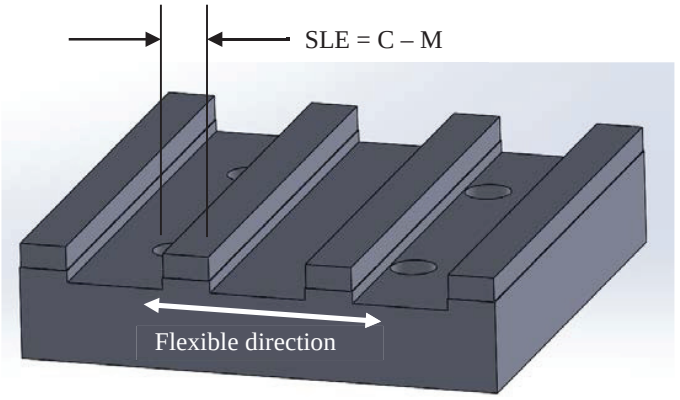

Fig. 7. The workpiece included four ribs that were initially machined to the same dimensions. The {5 mm axial depth, 2 mm radial depth} cuts were then performed on one edge at a different spindle speed for each rib. The SLE was calculated as the difference between the commanded, C, and measured, M, rib widths. The flexible direction for the flexure is identified.

The predicted and measured Poincaré maps for three of the 11 spindle speeds are presented in Figs. 8-10. Figure 8 displays the 3180 rpm results that exhibit period-2 behavior. Figures 9 and 10 both demonstrate stable behavior (3300 rpm and 3600 rpm, respectively). The vibration amplitude is larger in Fig. 10 because this spindle speed is nearer the first integer fraction of the resonant spindle speed (125.8·60/2 = 7548/2 = 3774 rpm). The forced vibration amplitude is therefore increased. This would be considered a “best” spindle speed in traditional analyses because it identifies the peak of the corresponding secondary Hopf stability lobe.

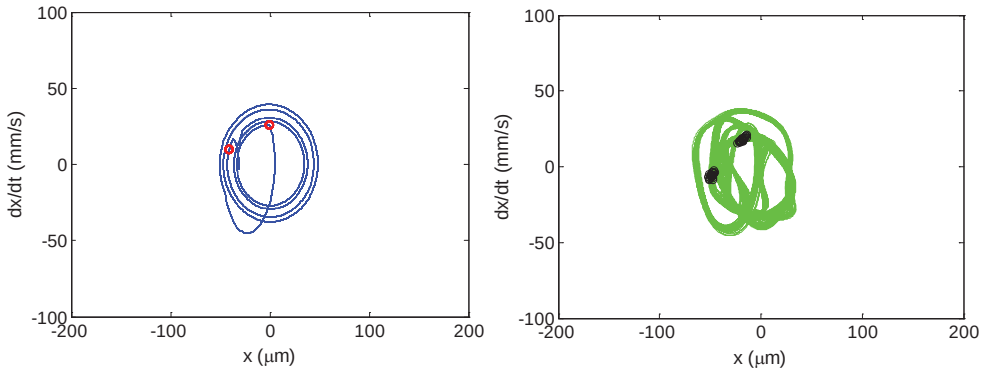

Fig. 8. Predicted (left) and measured (right) Poincaré maps for 3180 rpm. Period-2 behavior is seen. Note that *x* indicates the flexible direction for the flexure. The feed direction was *y* for these experiments.

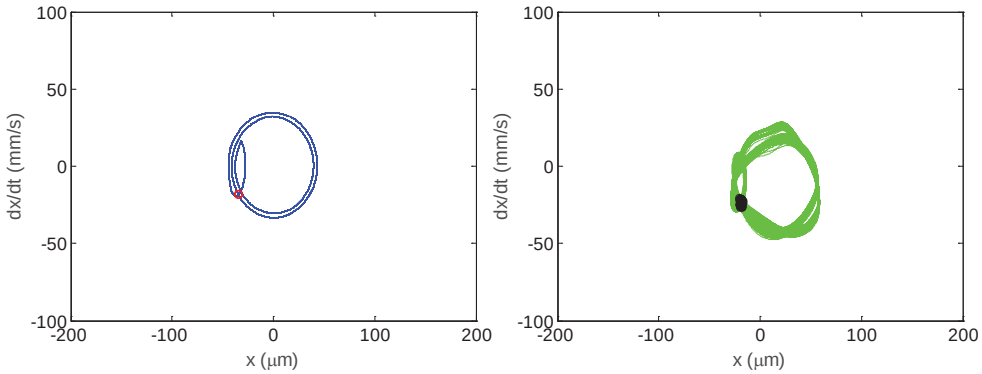

Fig. 9. Predicted (left) and measured (right) Poincaré maps for 3300 rpm. Stable behavior is seen.

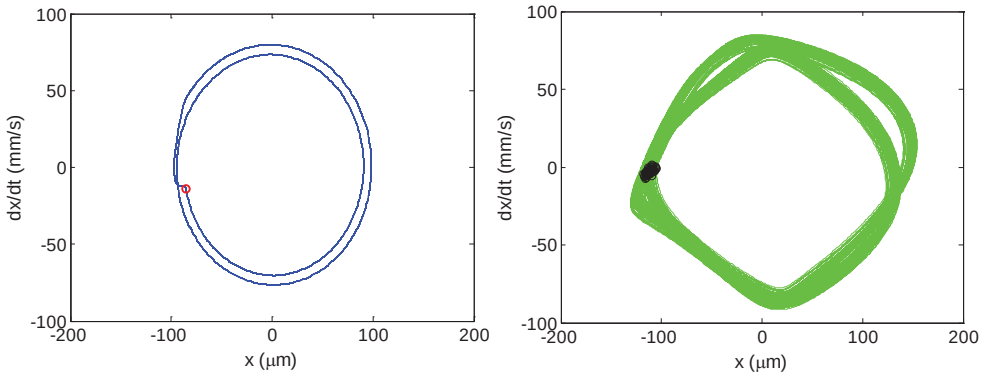

Fig. 10. Predicted (left) and measured (right) Poincaré maps for 3600 rpm. Stable behavior is seen with increased amplitude relative to 3300 rpm (Fig. 9).

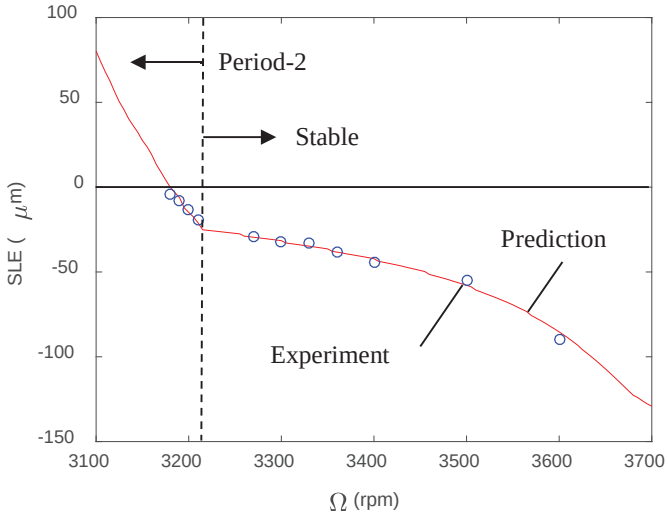

Fig. 11. SLE prediction from time domain simulation (line) and experimental results from rib cutting tests (circles). The four period-2 bifurcation tests are identified.

The SLE results are presented in Fig. 11. Four tests were completed under period-2 conditions and seven were performed under stable conditions. Good agreement is observed between prediction and measurement. The average error between prediction and measurement is 0.5 μm for the 11 tests.

The surface roughness was also measured using a scanning white light interferometer (ZeGage, Zygo Corporation). These results are presented in Table 2, where the Ra values were calculated from a line scan at the midpoint of the axial depth of cut extracted from the surface topography. The Ra is clearly larger for the period-2 conditions, where every other tool passage defines the surface roughness. The mean Ra for the period-2 conditions (four tests, 1.87 μm) is 5.2 times larger than the mean Ra for the stable conditions (seven tests, 0.36 μm).

Table 2. Surface roughness results for rib cutting tests.

Spindle speed (rpm)	Behavior	Ra (μm)	Spindle speed (rpm)	Behavior	Ra (μm)
3180	Period-2	1.76	3330	Stable	0.44
3190	Period-2	1.77	3360	Stable	0.34
3200	Period-2	1.87	3400	Stable	0.39
3210	Period-2	2.09	3500	Stable	0.36
3270	Stable	0.28	3600	Stable	0.35
3300	Stable	0.35			

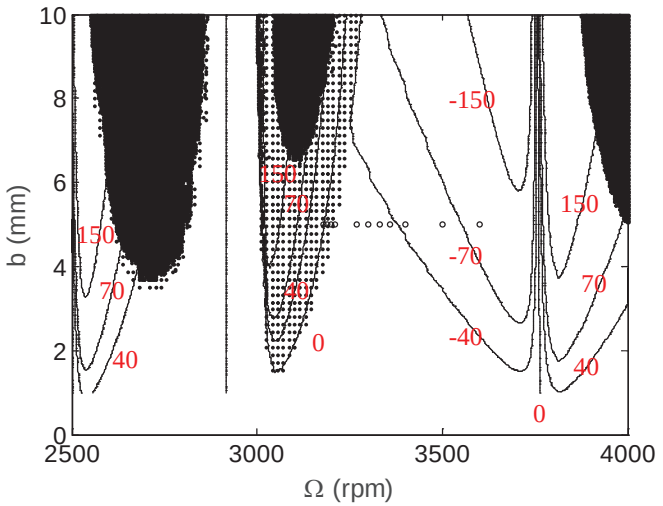

Fig. 12. Combined stability and SLE map for rib cutting process dynamics. The secondary Hopf instability is represented by the dark zone, the period-2 behavior is identified by the dotted zone, and the SLE is given by the contours (i.e., lines of constant SLE in μm).

The stability and SLE information is combined in Fig. 12. In this figure, the dark area represents secondary Hopf instability, the dotted area identifies the period-2 bifurcations, and the contour lines give the SLE in μm as a function of spindle speed (horizontal axis) and axial depth of cut (vertical axis). Zero SLE is seen near the traditional best speed of 3774 rpm. However, a steep gradient for small changes in spindle speed is also seen near this speed (i.e., the zero SLE contour is vertical). A zero SLE contour is also observed within the period-2 zone. Interestingly, the SLE gradient is not as steep within the period-2 zone as it is near the best speed at 3774 rpm. This also supports the possibility of producing acceptable parts under period-2 bifurcation machining conditions.

4. Conclusions

Surface location error and surface roughness predictions were completed using time domain simulation for both stable and period-2 milling conditions. The predictions were compared to experiment using a flexure-based platform with displacement and velocity metrology. It was observed that the simulation accurately predicted the milling performance using: 1) Poincaré maps, which plot the displacement versus velocity and are used to identify period-2 behavior via periodic sampling; 2) surface location error measurements completed using a coordinate measuring machine; and 3) surface roughness measurements carried out using a scanning white light interferometer. It was shown that the surface location error for period-2 (unstable) behavior follows similar trends observed for (stable) forced vibration, so zero or low error conditions may be selected even for period-2 bifurcation conditions. The surface roughness for the period-2 instability was seen to be larger than for stable conditions, although the final surface was still periodic. This increase in surface roughness occurs because the surface is defined by every other tooth passage and the apparent feed per tooth is increased.

Acknowledgements

This material is based on work supported by the National Science Foundation under Grant No. CMMI-1561221.

References

[1] Arnold, R. N. (1946). The mechanism of tool vibration in the cutting of steel, In: Proceedings of the Institute of Mechanical Engineers, 154.
[2] Doi, S. and Kato, S. (1956). Chatter vibration of lathe tools, Transactions of the ASME, 78: 1127-1134.
[3] Tobias, S. A. and Fishwick, W. (1958). The chatter of lathe tools under orthogonal cutting conditions, Transactions of the ASME, 80: 1079-1088.
[4] Tlusty, J. and Polacek, M. (1963). The stability of machine tools against self-excited vibrations in machining, In: Proceedings of the ASME International Research in Production Engineering Conference, Pittsburgh, PA, 465-474.
[5] Tobias, S. A. (1965). Machine Tool Vibration, Wiley, New York, NY.
[6] Merritt, H. E. (1965). Theory of self-excited machine-tool chatter, ASME Journal of Engineering for Industry, 87: 447-454.
[7] Shridar, R., Hohn, R. E., and Long, G. W. (1968). A general formulation of the milling process equation, ASME Journal of Engineering for Industry, 90: 317-324.
[8] Shridar, R., Hohn, R. E., and Long, G. W. (1968). A stability algorithm for the general milling process, ASME Journal of Engineering for Industry, 90: 330-334.
[9] Hanna, N. H. and Tobias, S. A. (1974). A theory of nonlinear regenerative chatter, ASME Journal of Engineering of Industry, 96: 247-255.
[10] Tlusty, J. and Ismail, F. (1981). Basic non-linearity in machining chatter, Annals of the CIRP, 30: 299-304.
[11] Minis, I. and Yanusevsky, R. (1993). A new theoretical approach for prediction of chatter in milling, ASME Journal of Engineering for Industry, 115: 1-8.
[12] Altintas, Y. and Budak, E. (1995). Analytical prediction of stability lobes in milling, Annals of the CIRP, 44(1): 357-362.
[13] Davies, M. A., Dutterer, B. S., Pratt, J. R., and Schaut, A. J. (1998). On the dynamics of high-speed milling with long, slender endmills. Annals of the CIRP, 47(1), 55-60.
[14] Stépán, G. and Kalmár-Nagy, T. (1997). Nonlinear regenerative machine tool vibrations, In: Proceedings of the 1997 ASME Design Engineering Technical conference on Vibration and Noise, Sacramento, CA, DETC 97/VIB-4021, 1-11.
[15] Mann, B.P., Bayly, P.V., Davies, M.A., and Halley, J.E. (2004). Limit cycles, bifurcations, and accuracy of the milling process, Journal of Sound and Vibration, 277: 31-48.
[16] Mann, B.P., Garg, N.K., Young, K.A., and Helvey, A.M. (2005). Milling bifurcations from structural asymmetry and nonlinear regeneration, Nonlinear Dynamics, 42(4): 319-337.
[17] Stépán, G., Szalai, R., Mann, B.P., Bayly, P.V., Insperger, T., Gradisek, J., and Govekar, E. (2005). Nonlinear dynamics of high-speed milling – Analyses, numerics, and experiments, Journal of Vibration and Acoustics, 127: 197-203.
[18] Moradi, H., Vossoughi, G., and Movahhedy, M. (2014). Bifurcation analysis of nonlinear milling process with tool wear and process damping: Sub-harmonic resonance under regenerative chatter, International Journal of Mechanical Sciences, 85: 1-19.
[19] Honeycutt, A. and Schmitz, T. (2015). The extended milling bifurcation diagram, Procedia Manufacturing, 1: 466-476.
[20] Honeycutt, A. and Schmitz, T. (2016). A numerical and experimental investigation of period-n bifurcations in milling, Journal of Manufacturing Science and Engineering, 139(1): 011003.
[21] Kline, W., DeVor, R., and Shareef, I. (1982). The prediction of surface accuracy in end milling, Journal of Engineering for Industry 104: 272-278.
[22] Tlusty, J. (1985). Effect of end milling deflections on accuracy, in: Handbook of High Speed Machining Technology (Ed. R.I. King), Chapman and Hall, New York, 140-153.

[23] Sutherland, J. and DeVor, R. (1986). An improved method for cutting force and surface error prediction in flexible end milling systems, Journal of Engineering for Industry, 108: 269-279.
[24] Montgomery, D. and Altintas, Y. (1991). Mechanism of cutting force and surface generation in dynamic milling, Journal of Engineering for Industry, 113(2): 160-168.
[25] Schmitz, T. and Ziegert, J. (1999). Examination of surface location error due to phasing of cutter vibrations, Precision Engineering, 23(1): 51–62.
[26] Yun, W.-S., Ko, J., Cho, D.-W., and Ehmann, K. (2002). Development of a virtual machining system, Part 2: prediction and analysis of a machined surface error, International Journal of Machine Tools and Manufacture, 42: 1607-1615.
[27] Schmitz, T. and Mann, B. (2006). Closed-form solutions for surface location error in milling, International Journal of Machine Tools and Manufacture, 46(12-13): 1369-1377.
[28] Schmitz, T., Couey, J., Marsh, E., Mauntler, N., and Hughes, D. (2007). Runout effects in milling: Surface finish, surface location error, and stability, International Journal of Machine Tools and Manufacture, 47(5): 841-851.
[29] Schmitz, T. and Smith, K.S. (2009). Machining Dynamics: Frequency Response to Improved Productivity, Springer, New York, NY.
[30] Smith, K.S. and Tlusty, J. (1991). An overview of modeling and simulation of the milling process, Journal of Engineering for Industry, 113: 169-175.
[31] Mann, B.P., Insperger, T., Bayly, P.V., and Stépán, G. (2003). Stability of up-milling and down-milling, Part 2: Experimental verification, International Journal of Machine Tools and Manufacture, 43(1): 35-40.
[32] Ransom, T., Honeycutt, A., and Schmitz, T. (2016). A new tunable dynamics platform for milling experiments, Precision Engineering, 44: 252-256.